# Retrieval of Surface Reflectance and LAI Mapping with Data from ALI, Hyperion and AVIRIS

P. Gong[1], G. Biging[1] , R. Pu[1], and M. R. Larrieu[2]

[1]Center for Assessment and Monitoring of
Forest and Environmental Resources (CAMFER)
University of California, Berkeley, USA
[2]Proyecto Forestal de Desarrollo, Secretaría de Apricultura
Buenos Aires, Argentina

# Contents

- Objectives
- Study Sites and Data
- Methods
- Results and Analysis
- Conclusions and Remarks
- Acknowledgments

# Objectives

- Develop a simple atmospheric correction method
- Map LAI with the ALI, Hyperion and AVIRIS
- Examine the capabilities of the three sensors for extracting LAI information
- Compare different VI and red-edge parameters for LAI estimation

# Study Sites and Data

- Study sites:
  - Two sites, in Patagonia, Argentina
  - Flat, semiarid region (show images)
  - Forest plantations, conifer species:PP, LP and Oregon P.
- Spectroradrometric measurements
  - ASD FieldSpec®Pro, covering 0.4 – 2.5 μm
  - Road surface, canopy of young plantation
- LAI measurements
  - 70 LAI plots, with LICOR LAI-2000 PCA
  - Effective LAI

# Study Sites and Data (Cont'd)

- ALI: Advanced Land Imager

  Multispectral, 9 bands, 1 panchromatic, 30 m, 3/27/2001
- Hyperion: Hyperspectral Imager
  - 220 bands, 0.4 – 2.5 μm
  - 10 nm spectral, 30 m spatial resolution, 3/27/2001
- AVIRIS: Airborne Visible/InfraRed Imaging Spectrometer
  - Hyperspectral sensor, altitude of 5029 m
  - 224 bands, 0.4 – 2.5 μm
  - 10 nm spectral, 3.6 m spatial resolution, 2/15/2001

# Study Sites (Cont'd)

- Part of the images over the two sites

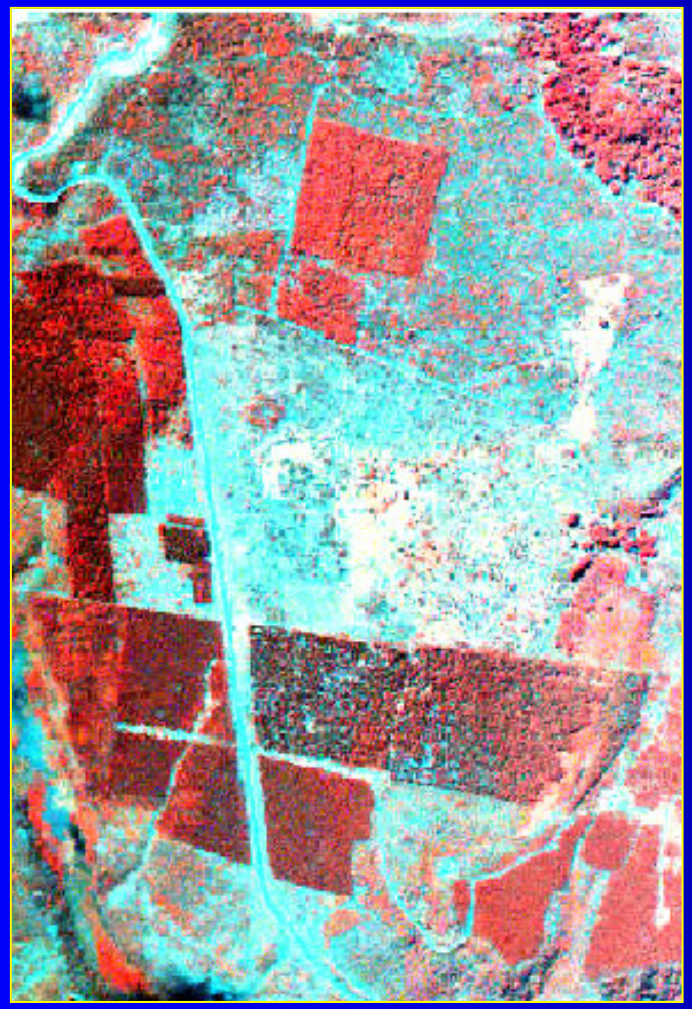

North

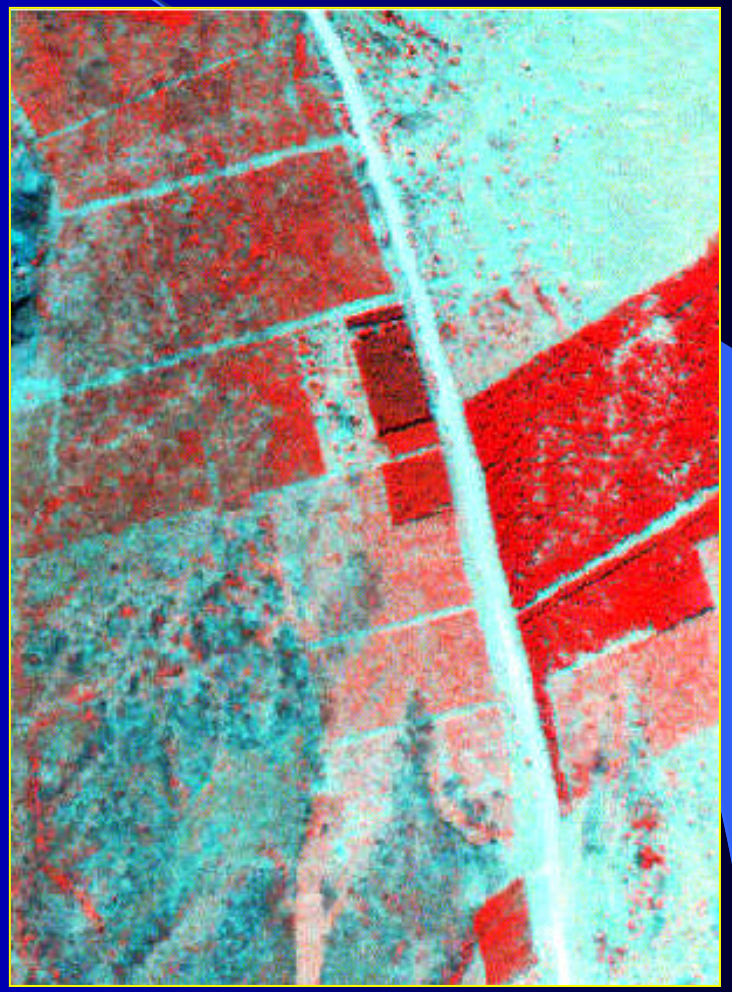

South

# Methods

- Atmospheric correction
  - Radiative transfer (RT) model
  - Radiance simulated with MODTRAN4
  - Retrieval surface reflectance
- LAI estimation and mapping
  - Correlation
  - LAI prediction model
  - LAI prediction and mapping

# Atmospheric correction: A flowchart

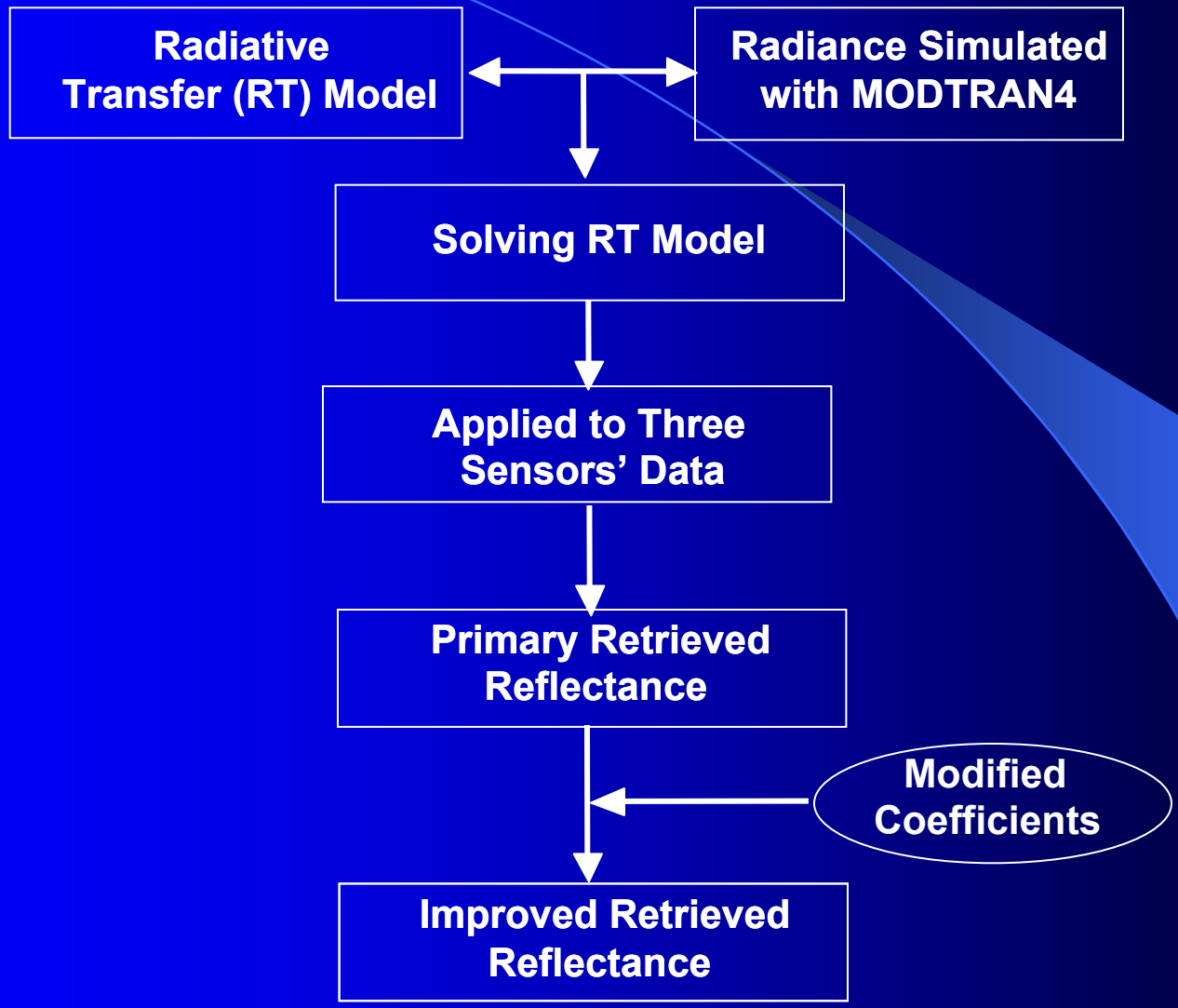

# RT model

The at-sensor radiance *L* can be related to the Lambertian surface reflectance ρ by

$$L = L_a + \frac{T_2 \rho}{1 - S\rho} \frac{E_0 \cos\theta_0}{\pi}$$

Where,

$L_a$ : atmospheric path radiance,

$T_2$ : two way transmittance for the sun-surface-sensor path,

$S$ : spherical albedo of the atmosphere,

$E_0$ : exoatmospheric solar irradiance, and

$\theta_0$ : solar zenith angle.

# Radiance simulation with MODTRAN4

- Input 3 surface reflectance values: 0.0, 0.3, 0.5
- Water vapor value 0.7 $cm/cm^{2,}$
- And other necessary parameters for the code
- Output total radiance

# Solving RT model

- To solve RT model, need 3 output total radiances simulated with MODTRAN4.
- Solve to obtain $L_a$, $T_2$, and $S$.

# Retrieval of surface reflectance of three sensors' data

- Retrieving surface reflectance: $\rho$ by RT model with known $L_{img}$, $L_a$, $T_2$, and $S$ for
  - *ALI*
  - *Hyperion*
  - *AVIRIS*

# Correlation analysis

- Extract pixel values at 32 LAI measured plots
  - From the retrieved reflectance images
  - 1-4 pixels at each LAI plot from Hyperion and ALI, 25-225 from AVIRIS
- General correlation analysis of spectral bands with LAIs
  - Correlograms of inter-band for Hyperion and AVIRIS
  - Correlation with 32 LAI measurements

# LAI prediction models and mapping

- Select a bunch of bands used for regression analysis based on
  - Correlograms of inter-band of the hyperspectral sensors' data
  - Peak values along the correlation curves
  - Physical meaning (absorption features)

  because of redundant information of and inflation phenomenon of $R^2$ of small observation size (32) relative to large number of bands (~200) of hyperspectral data. Select 12-15 bands from Hyperion and AVIRIS
- Constructing a 6-term LAI prediction model for the three sensors' data
- Predicting pixel-based LAI with 6-term prediction models for three sensors' data

# Results and Analysis

- Three total radiances simulated
- Results at different processing stages
- ASD ratio coefficients
- Comparison of retrieved reflectances from the three sensors
- Correlograms of inter-band of hyperspectral data
- Correlation of three sensors with ALI
- Determination of 6-term models
- LAI prediction model (Tables)
- LAI maps

# Three total radiances simulated by MODTRAN4, inputs: ref=0.0, 0.3, 0.5 and wv = 0.7 cm/cm$^2$

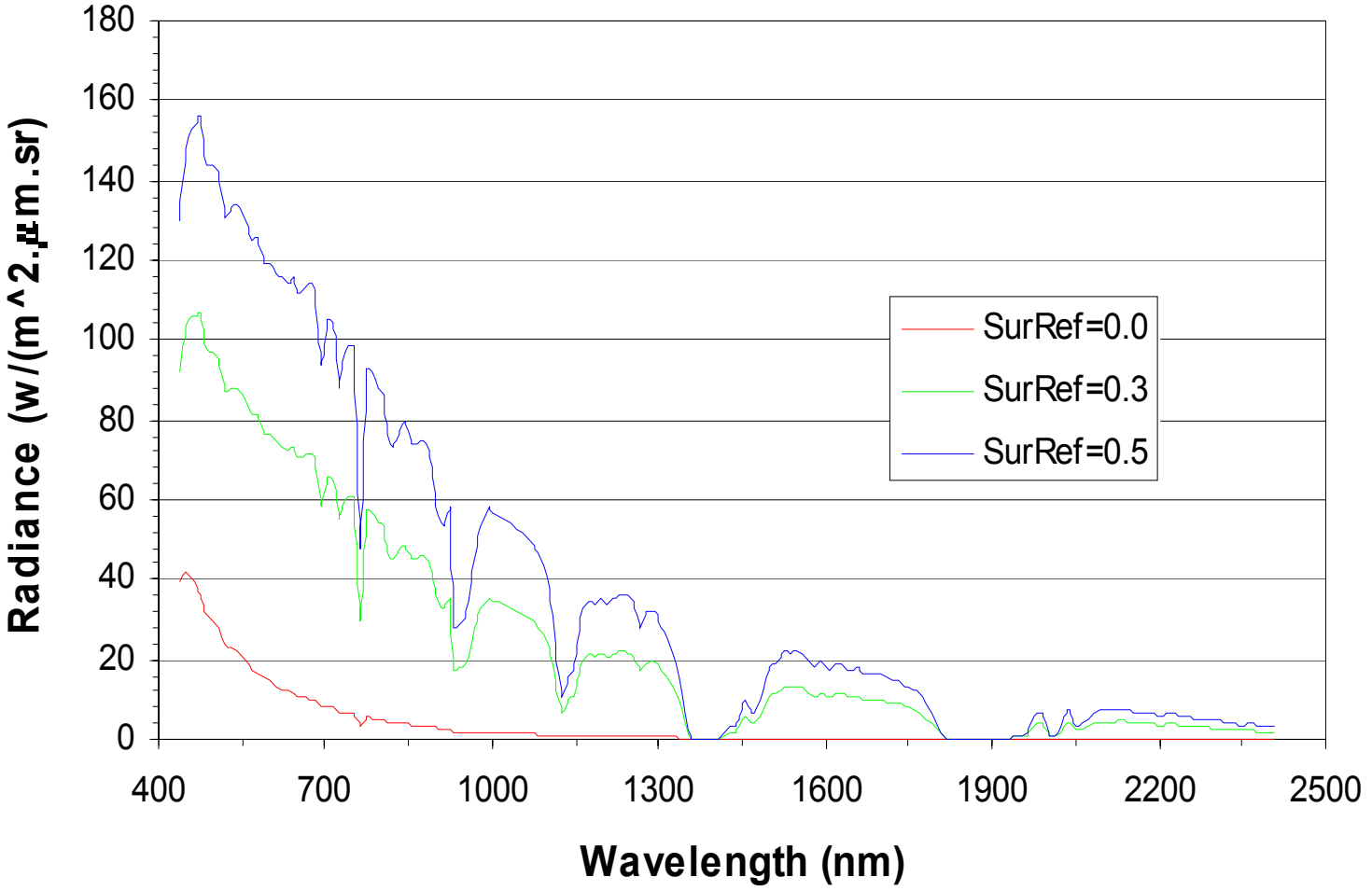

# Original radiance of Hyperion

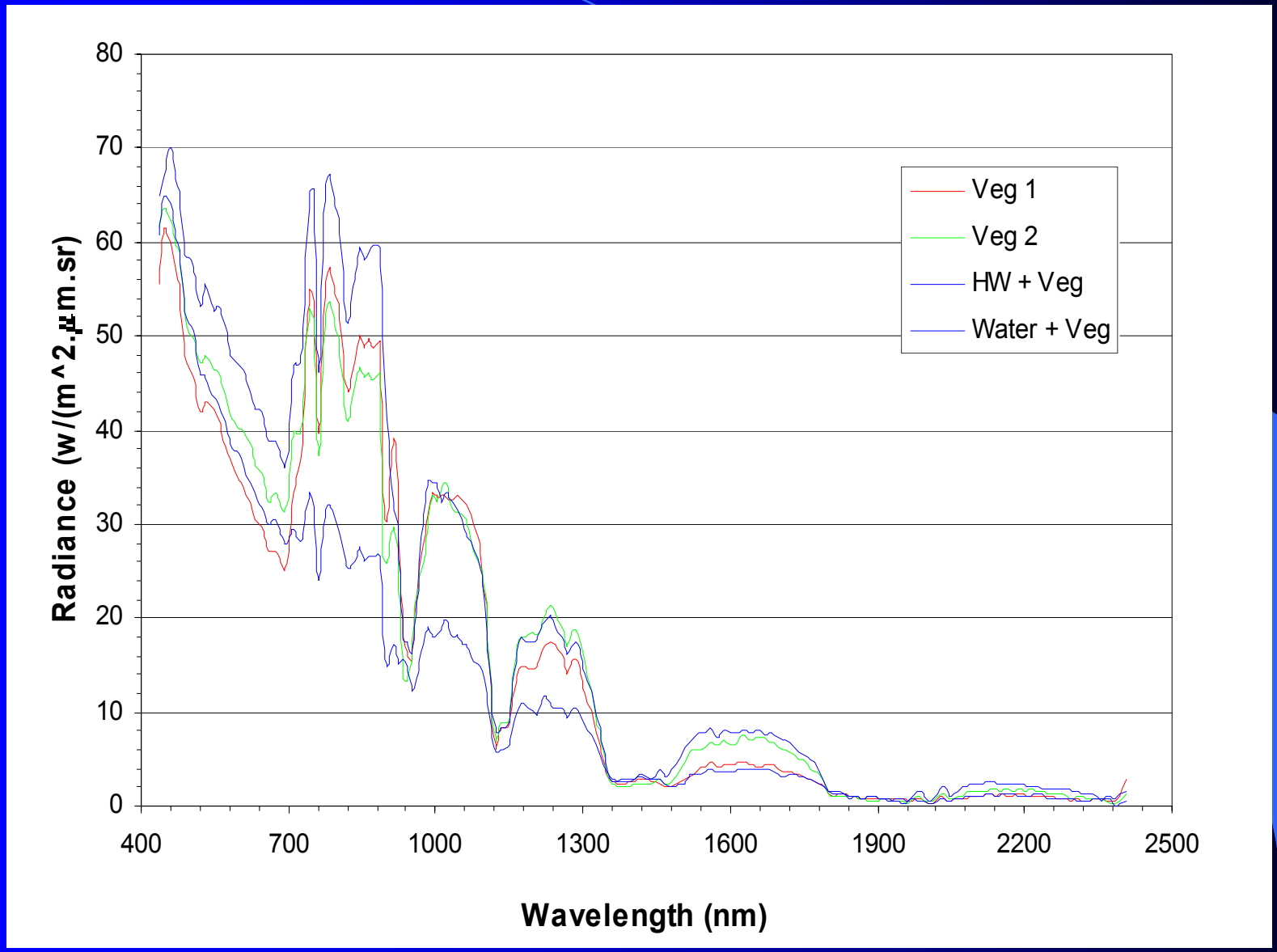

# Corrected radiance of Hyperion

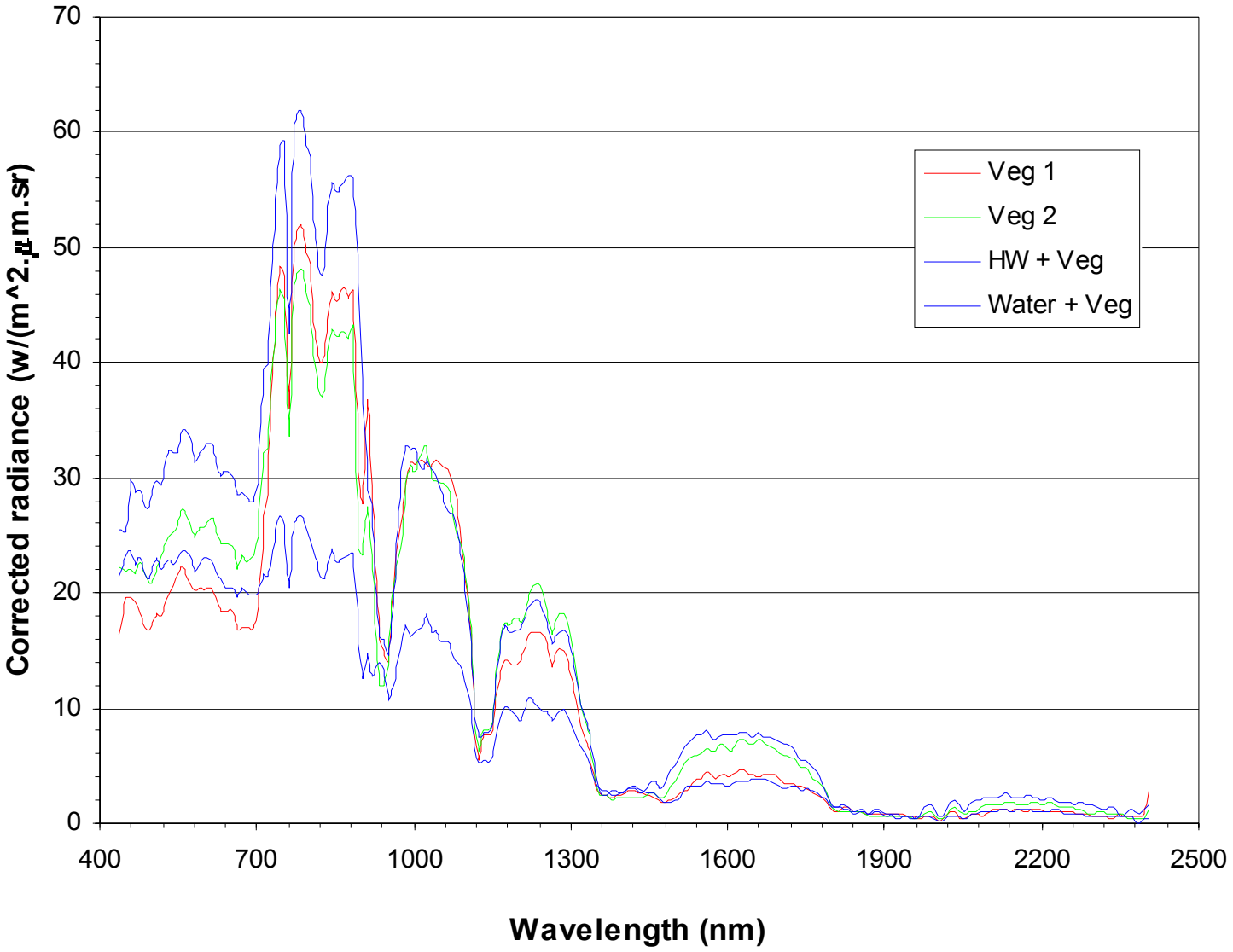

# Surface reflectance retrieved from Hyperion

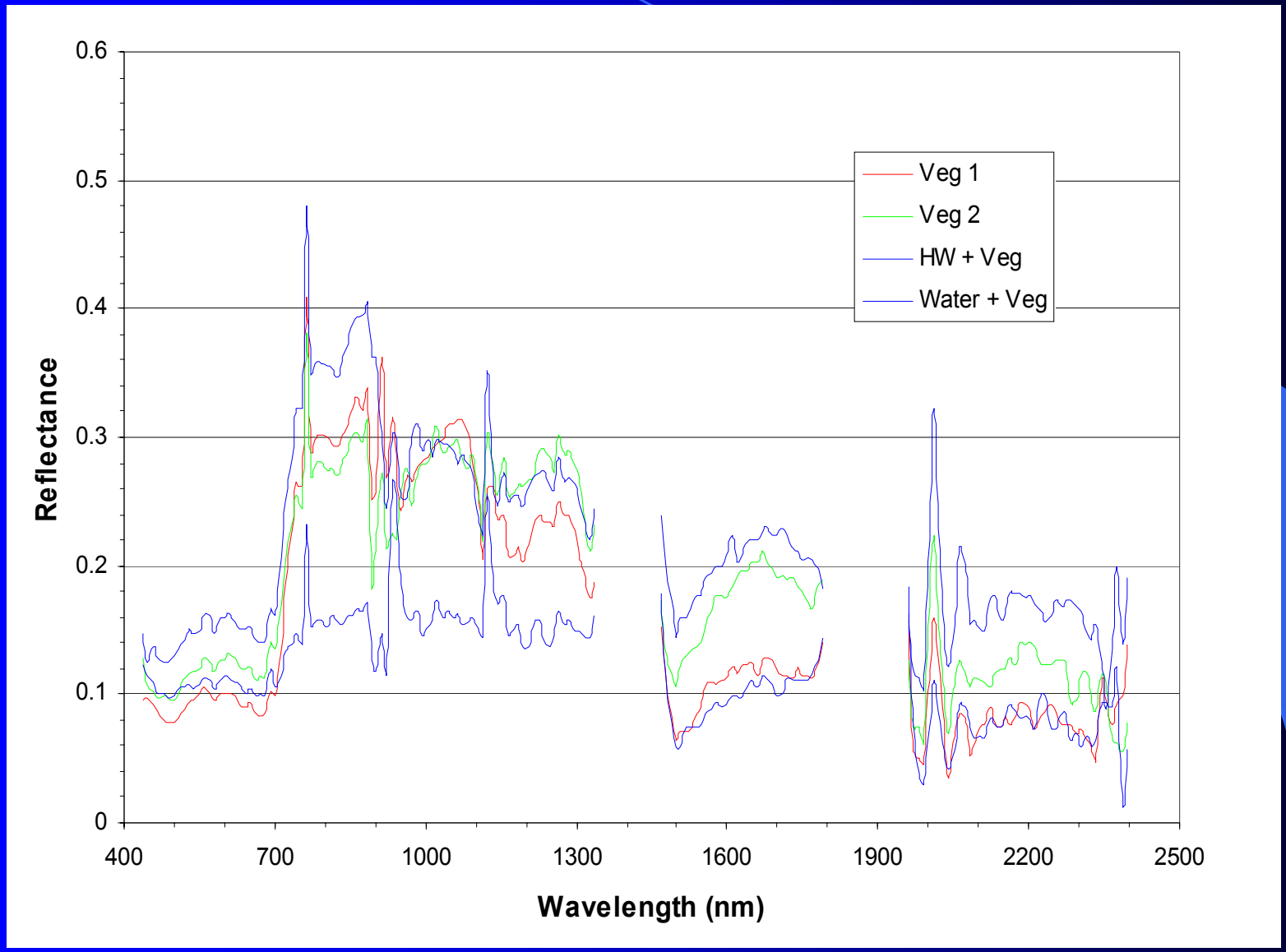

# Modified surface reflectance retrieved from Hyperion

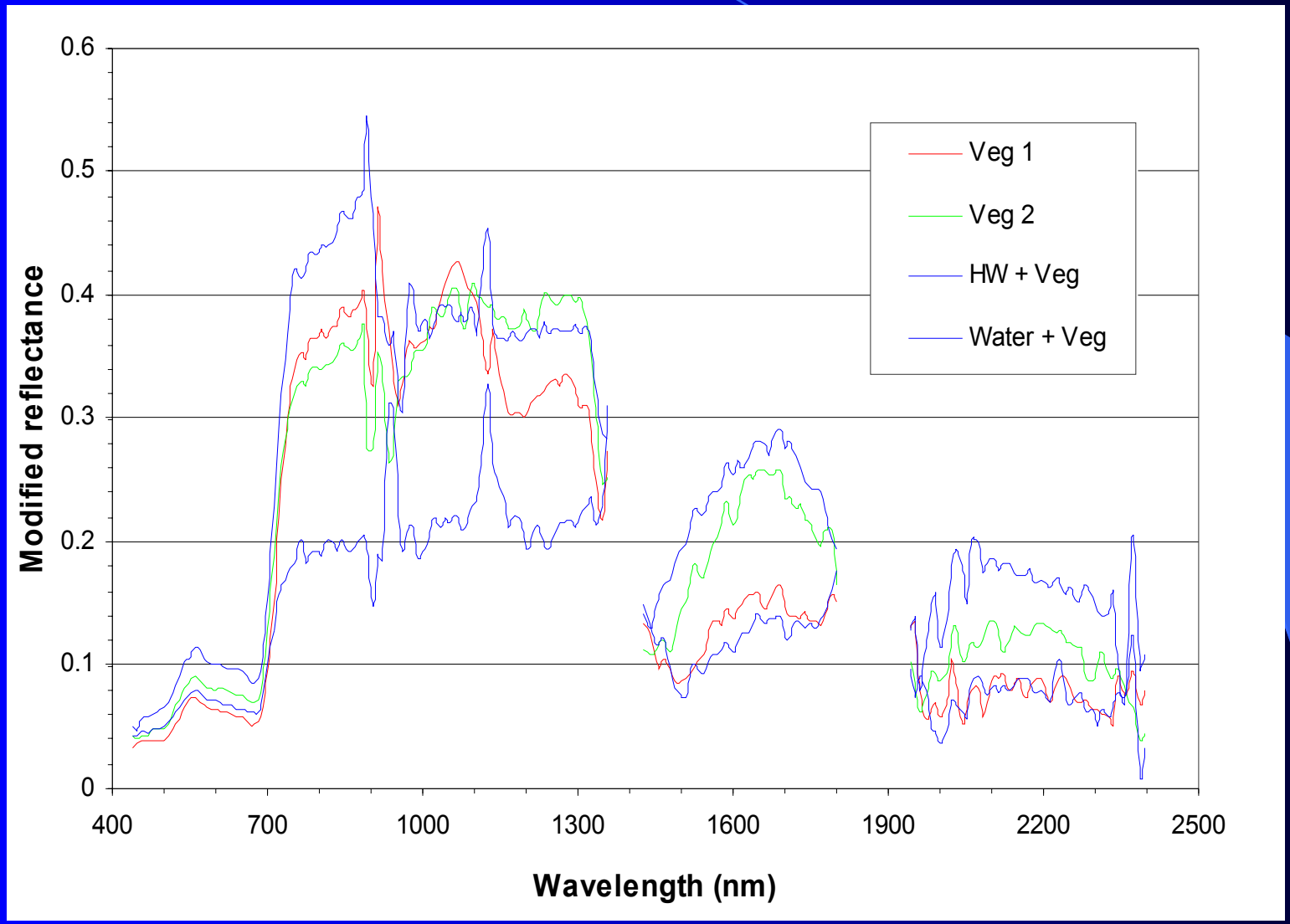

# ASD ratio coefficients

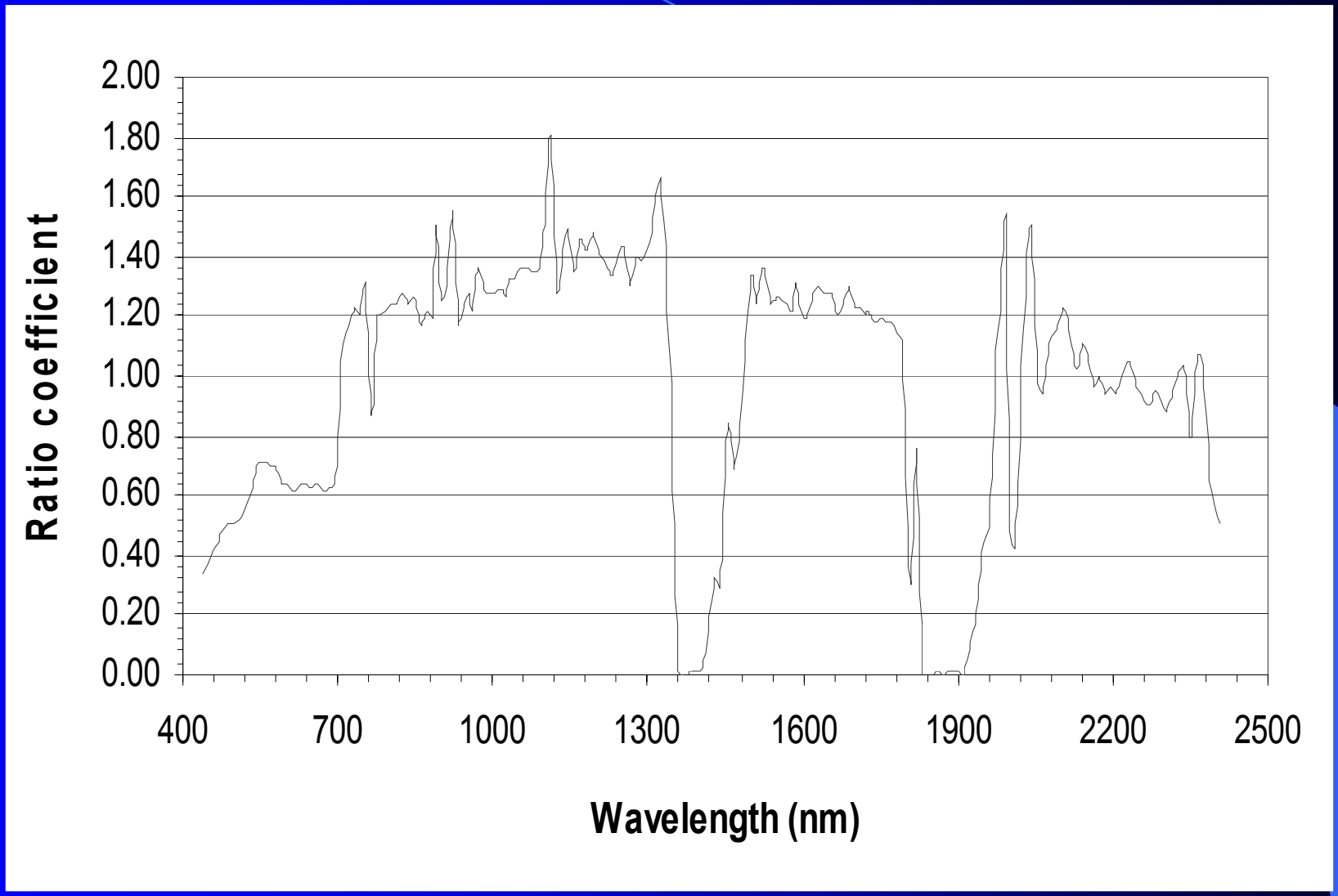

# Comparison of retrieved reflectances among three sensors: ALI, Hyperion and AVIRIS

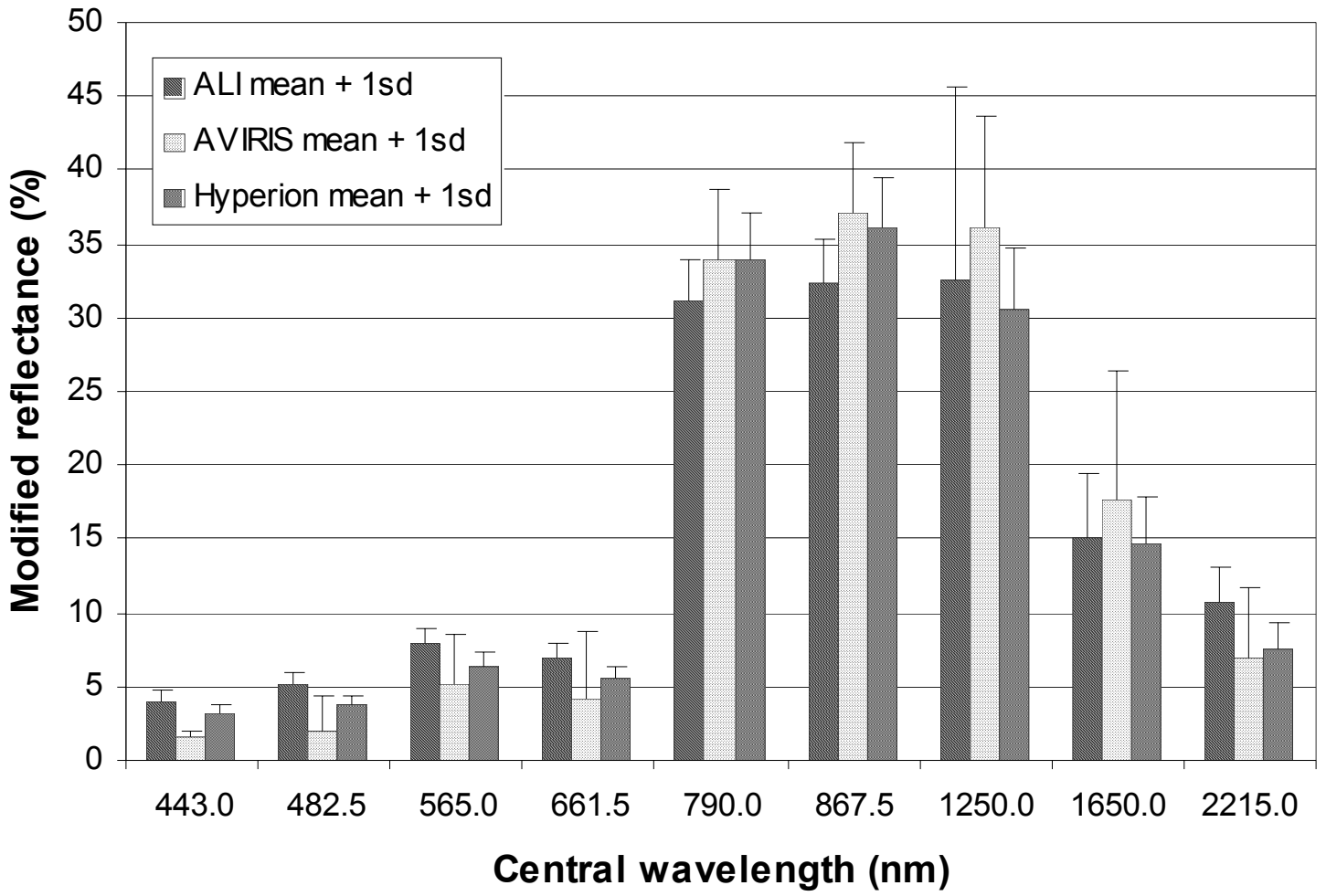

# Comparison of retrieved reflectances between two sensors: Hyperion and AVIRIS

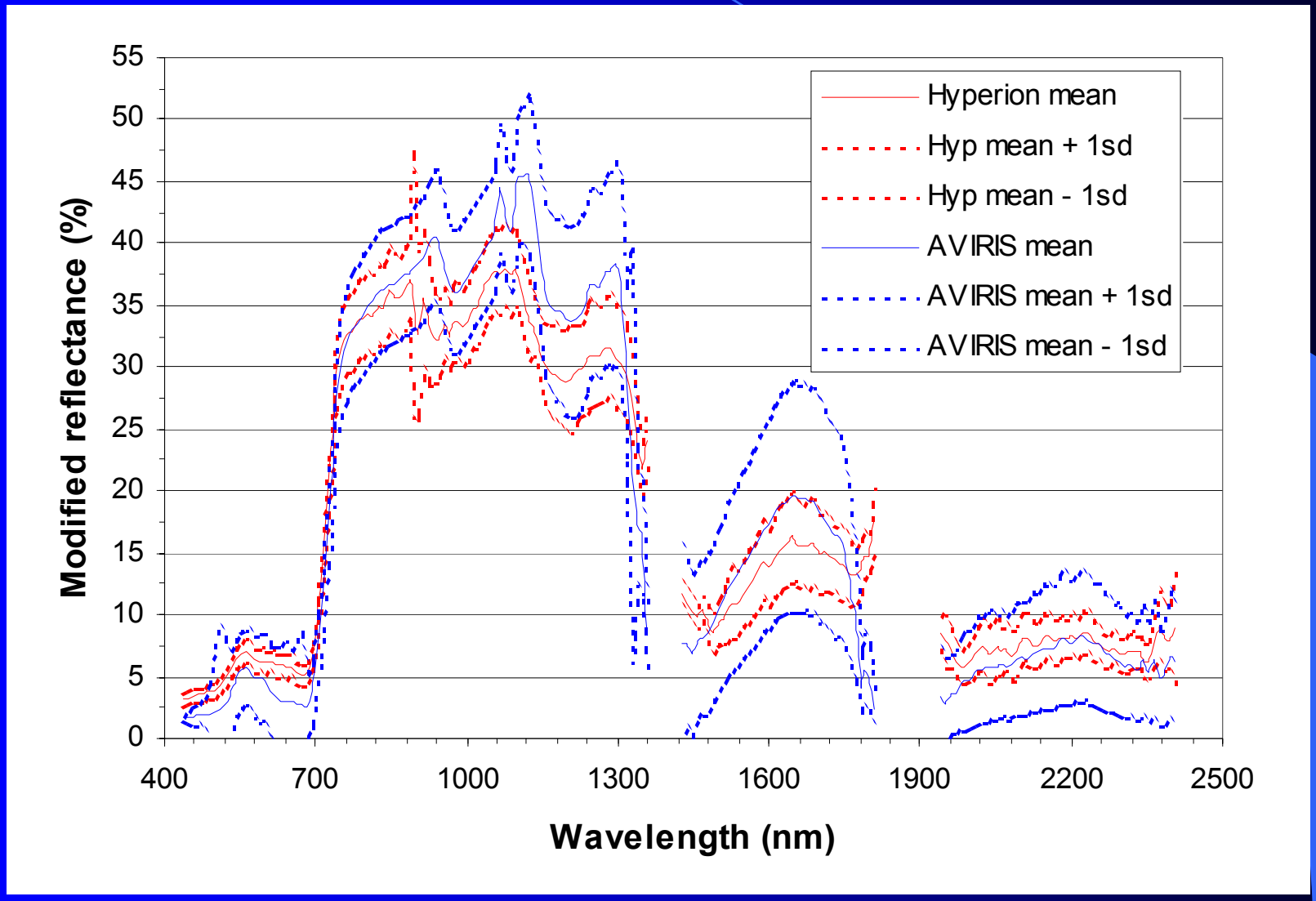

# Correlograms of inter-band

## Hyperion

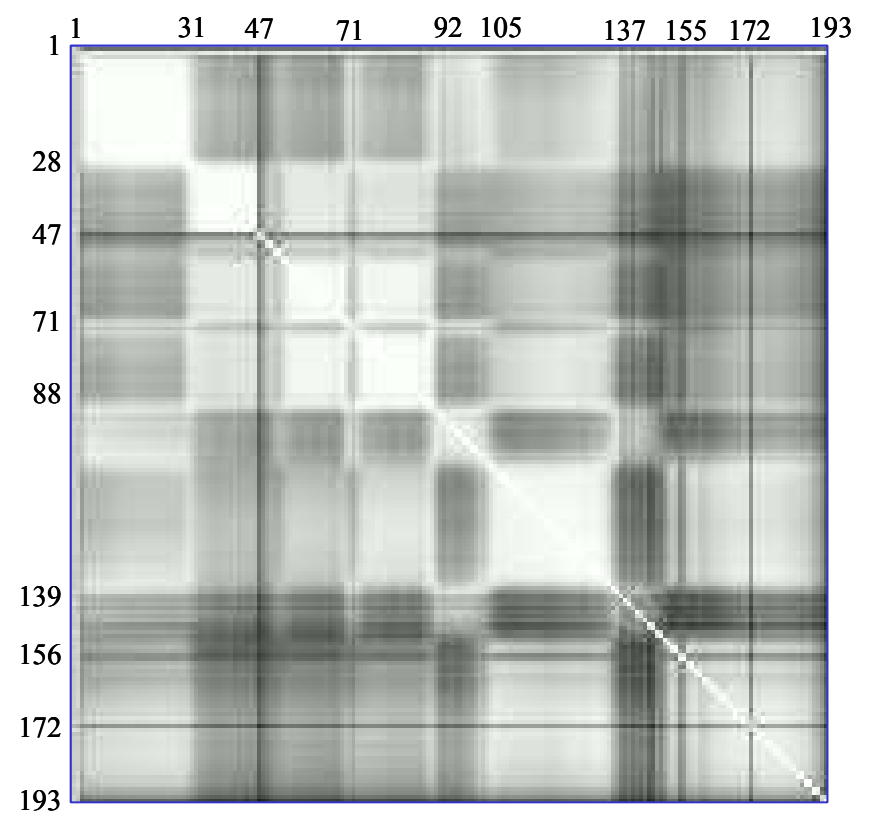


Correlogram of inter-band of Hyperion image, calculated in retrieved reflectance, 1-193 bands

## AVIRIS

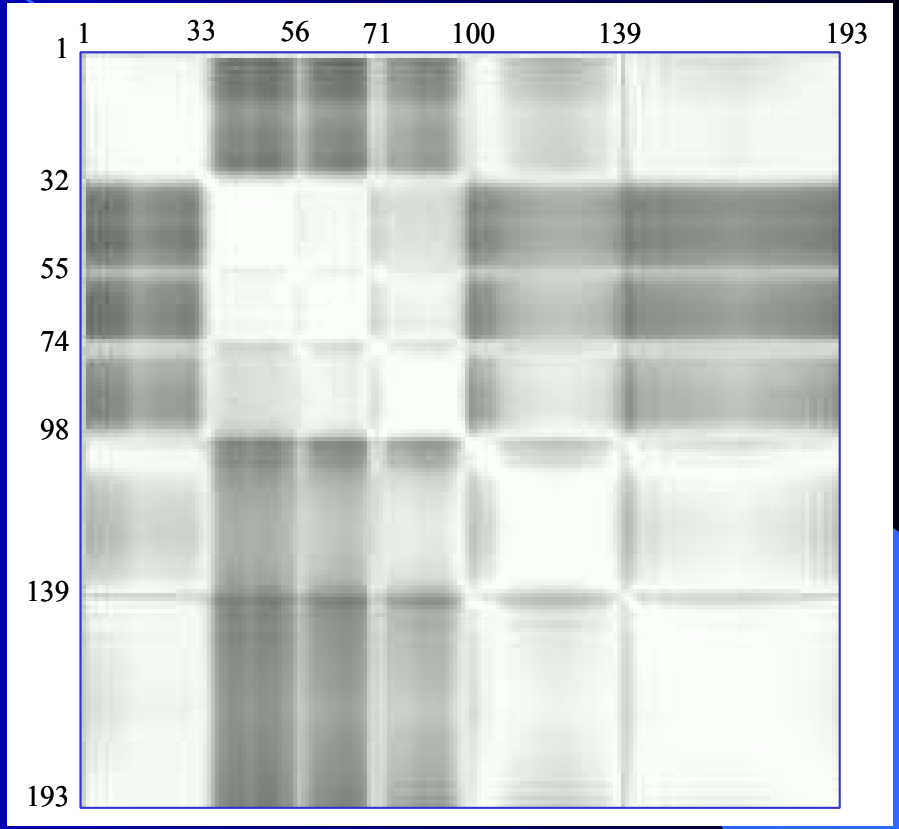


Correlogram of inter-band of AVIRIS image, calculated in retrieved reflectance, 1-193 bands

# Correlation coefficients of three sensors' data with LAI

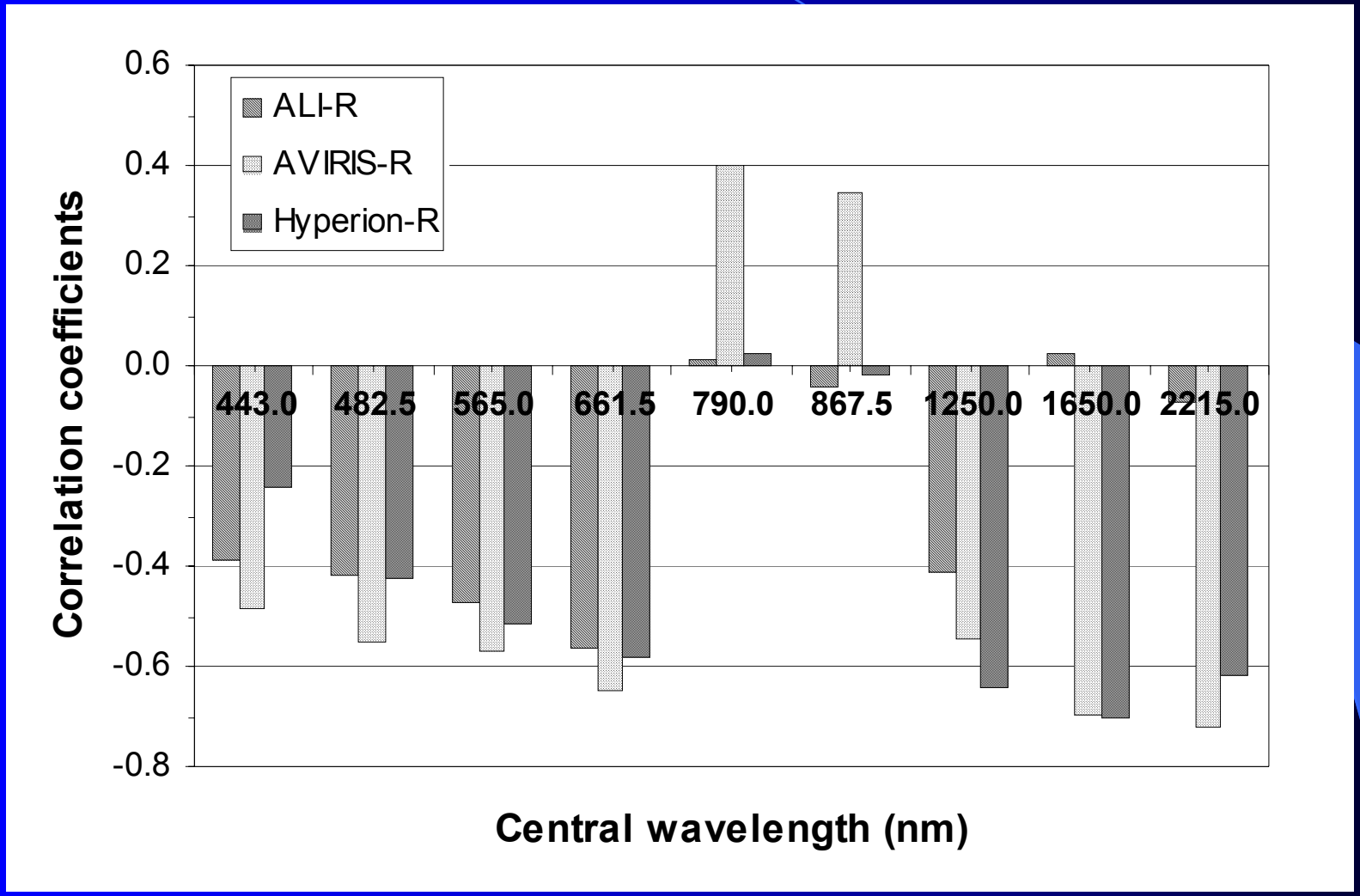

# Correlation coefficients of two sensors: Hyperion and AVIRIS with LAI

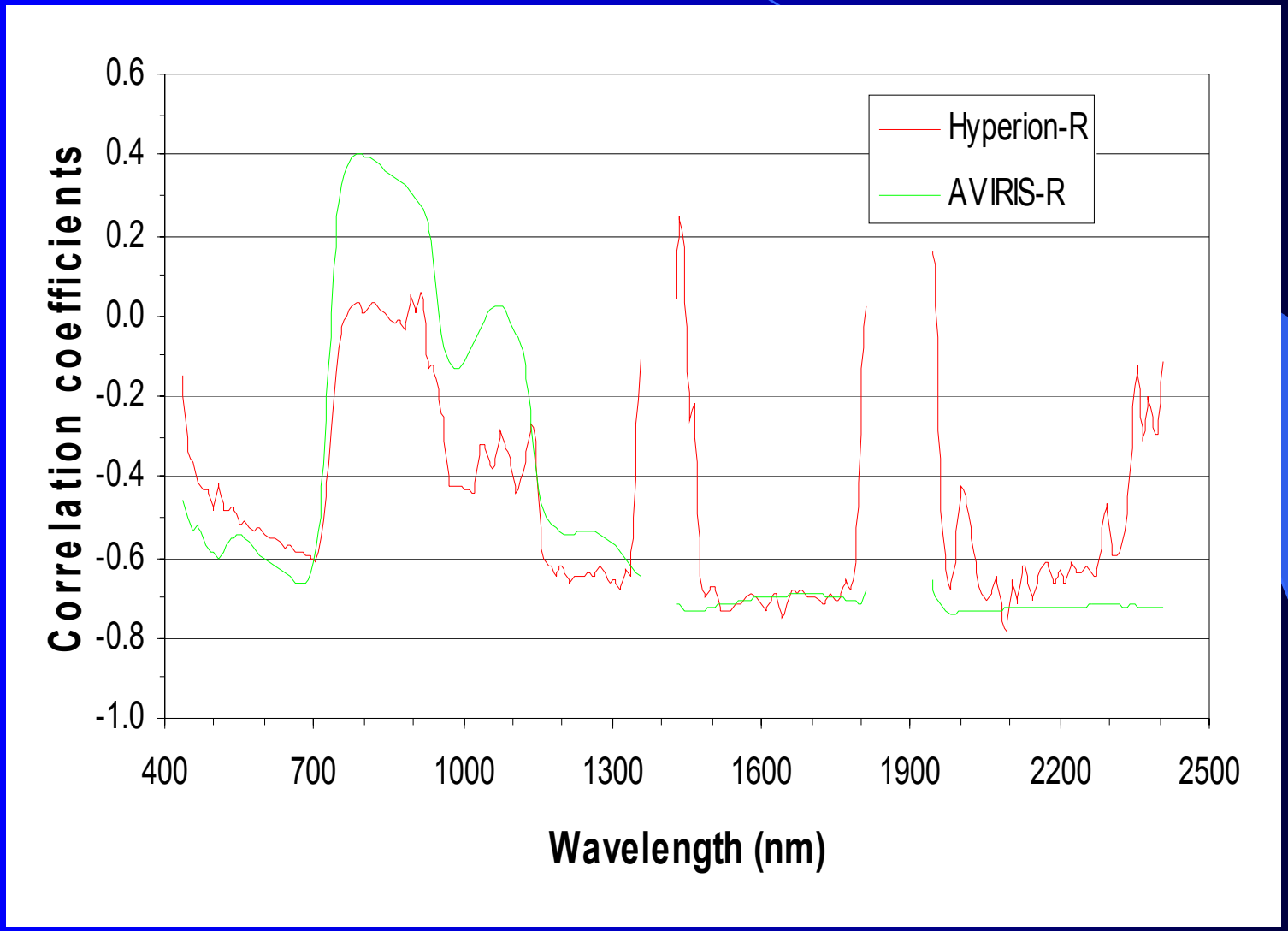

# Determination of 6 bands used for constructing LAI prediction models

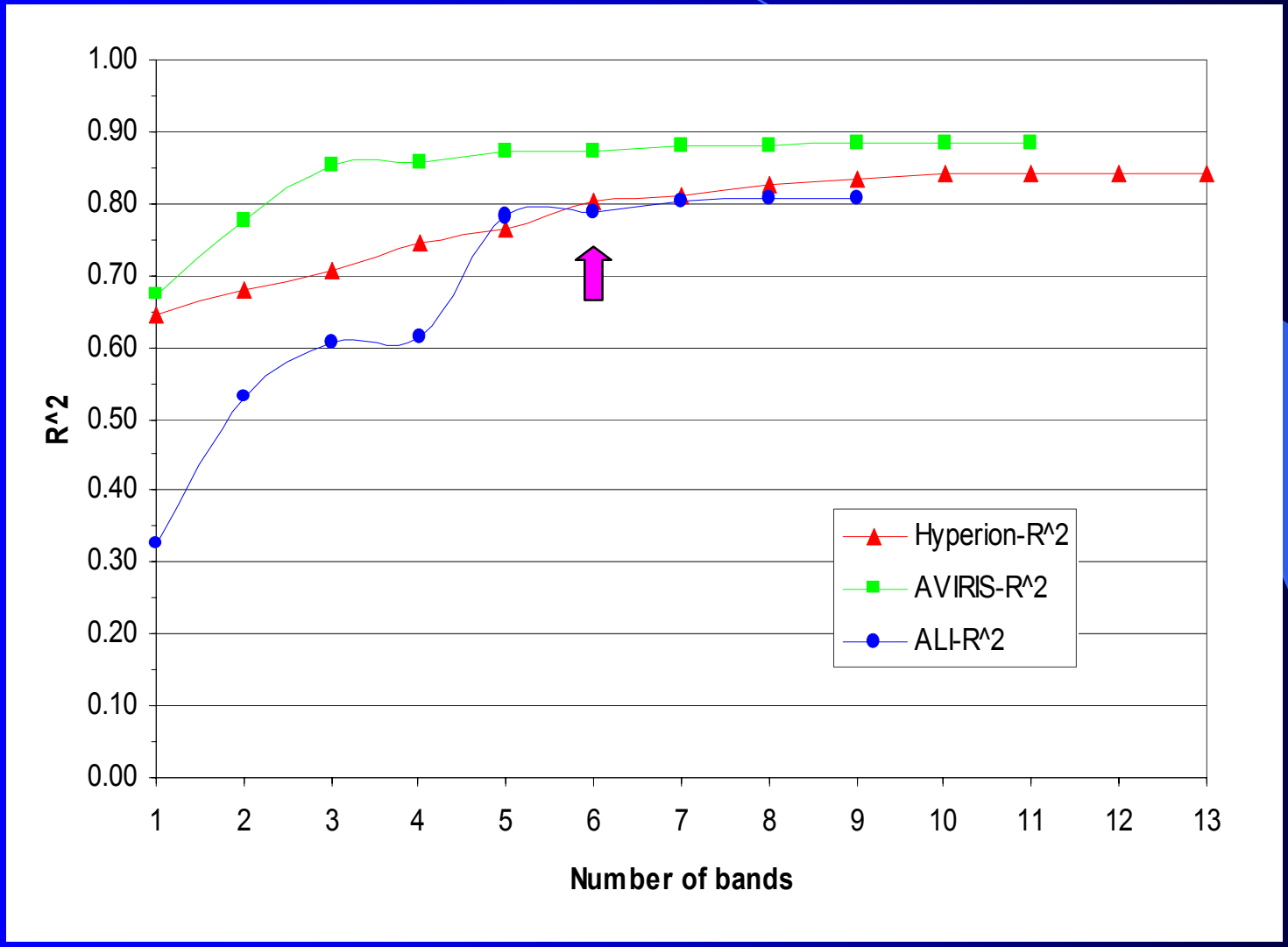

# LAI prediction models using retrieved surface reflectance data from ALI, Hyperion and AVIRIS N = 32, 6 bands selected into the models.

| | Hyperion | ALI | AVIRIS |
|---|---|---|---|
| | Log(Ref) | Log(Ref) | Log(Ref) |
| $R^2$ | 0.8019 | 0.7884 | 0.8731 |
| Wavelengths (nm) | 499, 913, 1437 1639, 2093, 2275 | 483, 790, 868 1250, 1650, 2215 | 684, 932, 1080 1991, 2261, 2400 |
| OAA(%) | 78.56 | 77.82 | 82.83 |
| S.D. | 0.5492 | 0.5679 | 0.4397 |

Note: OAA=overall accuracy; S.D.=standard deviation;
all of R2 are significant at 0.99 confident level.

# LAI maps

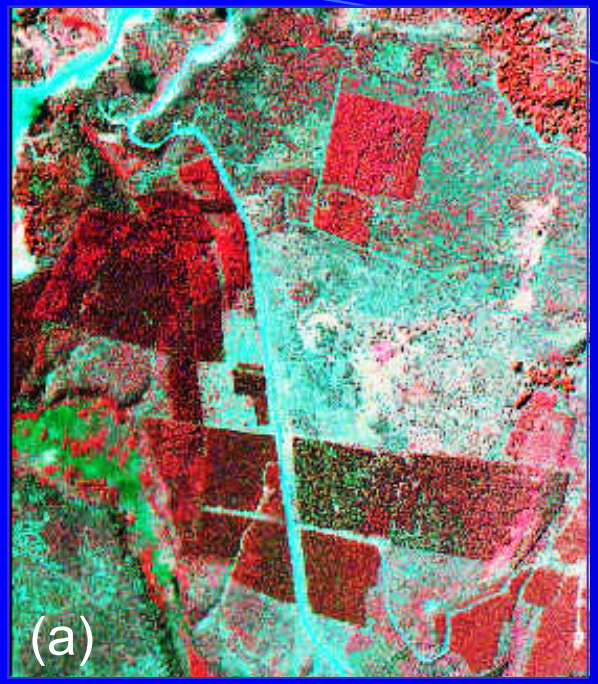



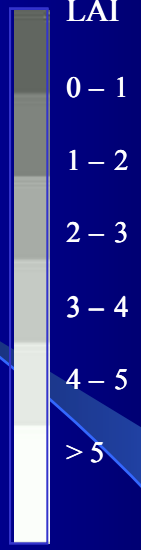


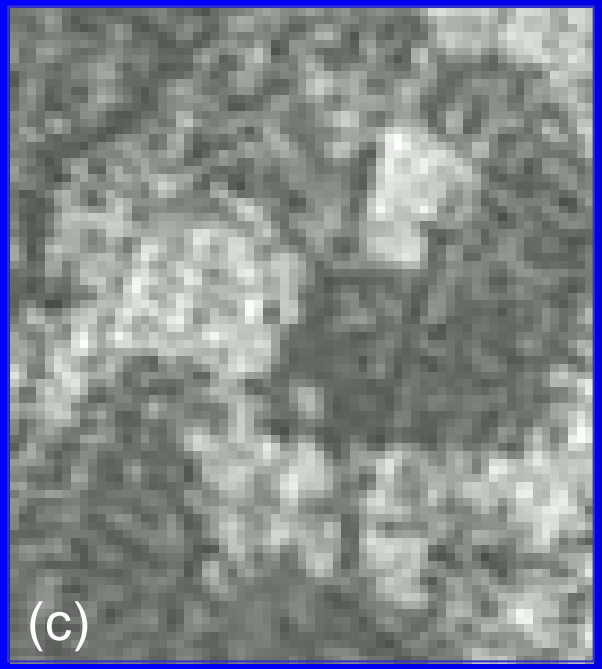


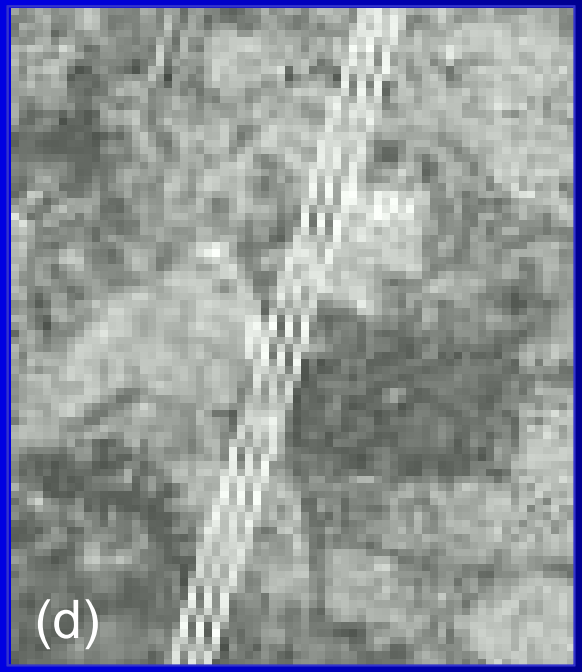


LAI maps, (a) pseudo-color composite of AVIRIS, (b) LAI map from AVIRIS, (c) LAI map from Hyperion and (d) LAI map from ALI

# 12 VIs

| Index | Formula | Description | References (e.g.) |
|---|---|---|---|
| SR | $\rho_{NIR} / \rho_R$ | Near-infrared / Red rreflectance ratio (Simple Ratio VI). Related to changes in amount of green biomass, pigment content and concentraion and leaf water stress etc. | Baret and Guyot, 1991; Tucher, 1979. |
| NDVI | $(\rho_{NIR} - \rho_R)/(\rho_{NIR} + \rho_R)$ | Normalized Difference Vegetation Index. Related to changes in amount of green biomass, pigment content and concentraion and leaf water stress etc. | Fassnacht et al., 1997; Smith et al., 1991. |
| PVI | $\frac{1}{\sqrt{a^2+1}}(\rho_{NIR} - a\rho_R - b)$ a = slope of the soil line b = soil line intercept | Perpendicular Vegetation Index, orthogonal to the soil line. Attempts to eliminate differences in soil background and is most effective under conditions of low LAI, applicable for arid and semiarid regions. | Baret and Guyot, 1991; Huete et al., 1985. |
| SAVI | $\frac{(\rho_{NIR} - \rho_R)(1+L)}{(\rho_{NIR} + \rho_R + L)}$ L = a correction factor | Soil Adjusted Vegetation Index. L ranges from 0 for very high vegetation cover to 1 for very low vegetation cover; minimizes soil brightness-induced variations L=0.5 can reduce soil noise problems for a wide range of LAI. | Huete, 1988; Leeuwen and Huete, 1996. |
| NLI | $(\rho_{NIR}^2 - \rho_R)/(\rho_{NIR}^2 + \rho_R)$ | Non-Linear vegetation Index. Consider the relationship between many VIs and surface biophysical parameters is often nonlinear, and NLI linearizes relationships with surface parameters that tend to be nonlinear. | Goel and Qin, 1994 |
| RDVI | $(\rho_{NIR} - \rho_R)/(\rho_{NIR} + \rho_R)^{1/2}$ | Renomalized Difference Vegetation Index. RDVI linearizes relationships with surface parameters that tend to be nonlinear. | Roujean and Breon, 1995. |
| MSR | $\frac{(\rho_{NIR} / \rho_R - 1)}{(\rho_{NIR} / \rho_R)^{1/2} + 1}$ | Modified Simple Ratio. It can be an improvement over RDVI for linearizing the relationships between the index and biophysical parameters. | Chen, 1996. |

# 12 VIs (Cont'd)

| Index | Formula | Description | References (e.g.) |
|---|---|---|---|
| WDVI | $\rho_{NIR} - a\rho_R$<br>a = slope of the soil line | Weighted Difference Vegetation Index. WDVI assumes that the ratio between NIR and R reflectances of bare soil is constant; it is a mathematically version of PVI, but it has an unrestricted range. | Clevers, 1988; Clevers, 1991. |
| MNLI | $\frac{(\rho_{NIR}^2 - \rho_R)(1+L)}{(\rho_{NIR}^2 + \rho_R + L)}$<br>L = a correction factor | Modified Non-linear vegetation Index. MNLI is an improved version of NLI, and it also consider merit of SAVI. L=0.5 may be applicable for a wide range of LAI. For detailed description, see text. | Developed in this paper. |
| NDVI*SR | $\frac{(\rho_{NIR}^2 - \rho_R)}{(\rho_{NIR} + \rho_R^2)}$ | Attemps to combine merit of NDVI with that of SR. For detailed description, see text. | Developed in this paper. |
| SAVI*SR | $\frac{(\rho_{NIR}^2 - \rho_R)}{(\rho_{NIR} + \rho_R + L)\rho_R}$ | Attemps to combine merit of SAVI with that of SR. For detailed description, see text. | Developed in this paper. |
| TSAVI | $\frac{a(\rho_{NIR} - a\rho_R - b)}{[a\rho_{NIR} + \rho_R - ab + X(1+a^2)]}$<br>a = slope of the soil line<br>b = soil line intercept<br>X = adjustment factor to minimize soil noise. | Transformed Soil Adjusted Vegetation Index. Modify Huete (1988) SAVI to compensate for soil variability due to changes in solar elevation and canopy structure. | Baret and Guyot, 1991; |

Note: $\rho_R$ and $\rho_{NIR}$ enoted as reflectances in red and near-infrared wavelengths, but in this study, they represent band 1 and band 2 across all avaliable 193 bands of Hyperion data.

# Three approaches (Cont'd)

- Polynomial fitting (in fifth order)

$$\rho = a_0 + \sum_{i=1}^{5} a_i \lambda^i$$

- IG red edge model, linear fitting with least square solution (Miller et al., 1990)

$$R(\lambda) = R_s - (R_s - R_0)\exp\left(\frac{-(\lambda_0 - \lambda)^2}{2\sigma^2}\right)$$

# $R^2$ gray scale plot for SAVI vs. LAI

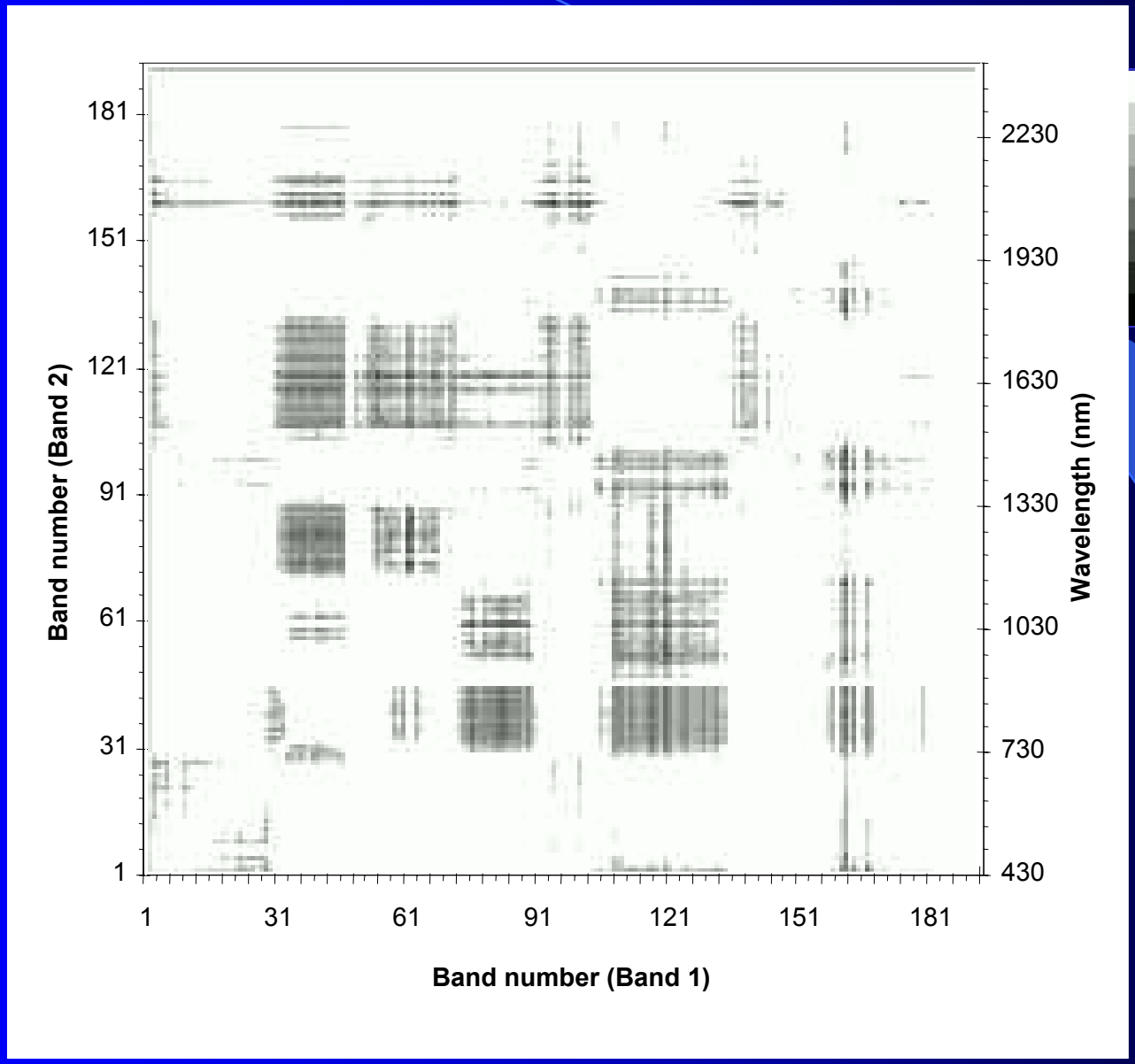

# Potential hyperspectral bands for estimating forest LAI

| Indiex | $R^2$ NIR-R/Optim. | Band center (nm) | Bandwidth (nm) | Band description (spectral region and possible absorption features) |
|---|---|---|---|---|
| SR | 0.55/0.70 | 825 | 140 | NIR region, **cell structure** multi-reflected spectra. |
| | | 1038 | 230 | NIR-SWIR region, **water**, **proten**, lignin, starch & oil absorption |
| | | 1250 | 180 | SWIR region, **water**, cellulose, starch and lignin absorption |
| | | 1648 | 290 | SWIR region, **protein**, **nitrogen**, **lignin**, **cellulose**, sugar, starch absorption. |
| NDVI | 0.55/0.70 | … | … | 4 bands similar to SR's |
| PVI | 0.45/0.64 | 814 | 140 | NIR region, **cell structure** multi-reflected spectra. |
| | | 1050 | 100 | NIR-SWIR region, **proten**, lignin, and oil absorption |
| | | 1250 | 190 | SWIR region, **water**, cellulose, starch and lignin absorption |
| | | 2100 | 10 | SWIR region, **starch,** cellulose absorption |
| SAVI | 0.50/0.67 | … | … | 4 bands similar to NDVI's or SR's |
| NLI | 0.50/0.73 | 821 | 157 | NIR region, **cell structure** multi-reflected spectra. |
| | | 1200 | 578 | NIR-SWIR region, **water**, proten, starch, lignin, cellulose, and oil absorption |
| | | 1250 | 191 | SWIR region, **water**, cellulose, starch and lignin absorption |
| | | 1640 | 300 | SWIR region, **protein**, **nitrogen**, **lignin**, **cellulose**, sugar, starch absorption. |
| RDVI | 0.45/0.66 | 810 | 170 | NIR region, **cell structure** multi-reflected spectra. |
| | | 1054 | 10 | SWIR region, lignin and oil absorption |
| | | 1255 | 161 | SWIR region, **water**, cellulose, starch and lignin absorption |
| | | 1669 | 10 | SWIR region, lignin and starch absorption |
| | | 2093 | 10 | SWIR region, starch and cellulose absorption |

# Potential hyperspectral bands for estimating forest LAI (Cont'd)

| Indiex | $R^2$ NIR-R/Optim. | Band center (nm) | Bandwidth (nm) | Band description (spectral region and possible absorption features) |
|---|---|---|---|---|
| MSR | 0.50/0.70 | … | … | 4 bands similar to NDVI's or SR's |
| WDVI | 0.45/0.63 | 1377 | 10 | SWIR region, **water** absorption |
| | | 1427 | 10 | SWIR region, lignin absorption |
| | | 1639 | 10 | SWIR region,non apparent absorption |
| | | 2113 | 10 | SWIR region, **starch** and cellulose absorption |
| | | 2285 | 30 | SWIR region, starch, cellulose and protein absorption |
| MNLI | 0.45/0.75 | … | … | 4 bands similar to NLIs |
| NDVI*SR | 0.50/0.71 | … | … | 4 bands similar to NDVI's or SR's, but |
| SAVI*SR | 0.50/0.71 | … | … | 1 - 4 bands similar to SAVI's or SR's |
| | | 2083 | 30 | SWIR region, sugar, starch and cellulose absorption |
| | | 2153 | 10 | SWIR region, protein absorption |
| TSAVI | 0.50/0.71 | 832 | 120 | NIR region, **cell structure** multi-reflected spectra. |
| | | 1038 | 150 | NIR-SWIR region, **water**, **proten**, lignin, starch & oil absorption |
| | | 1240 | 170 | SWIR region, **water**, lignin, cellulose and starch absorption |
| | | 1660 | 260 | SWIR region, **lignin**, **cellulose, sugar**, starch, protein, and nitrogen absorption. |
| | | 2108 | 20 | SWIR region, **starch**, cellulose and protein absorption |

Note: Optim. = optimal correlation $R^2$; **bold chemicals** are principal for the absorption features

# 4-point approach

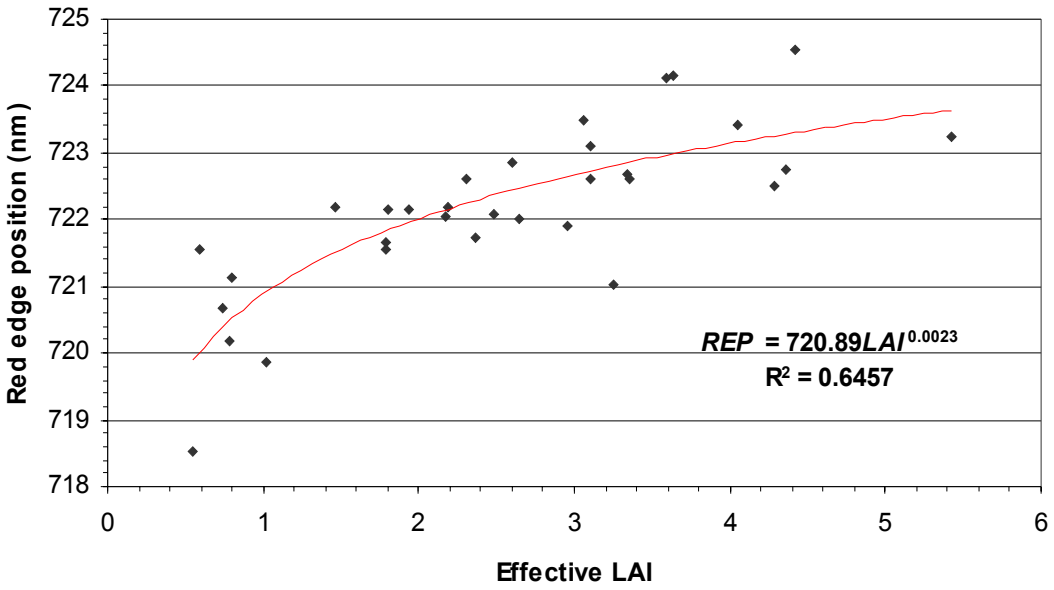


Forest LAI vs. two red edge parameters extracted with 4-point interpolating approach (using bands 671.62, 702.12, 742.80, and 783.48 nm). Upper: LAI versus red edge position; right: LAI versus red well (minimum reflectance position)

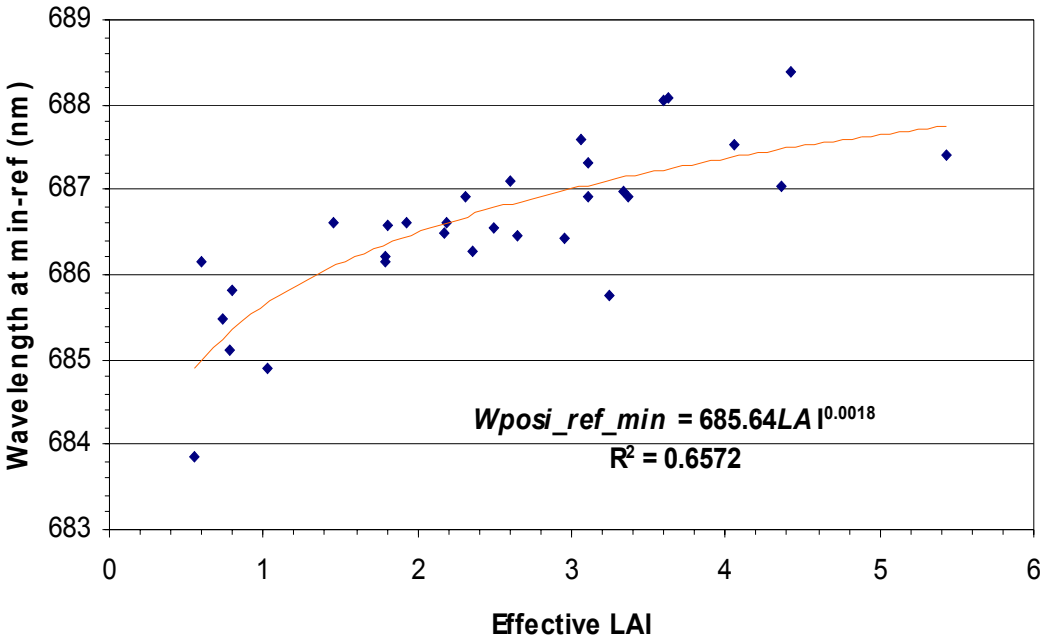

# Conclusions

- The method of atmospheric correction used in this study is promising but needs refinement.
- LAI prediction model derived from AVIRIS has the highest correlation and lowest regression SD, followed by Hyperion and ALI
- Since atmospheric effects on VNIR more than SWIR, more potential in SWIR with Hyperion.
- Atmospheric correction is critical for hyperspectral data application, especially in VNIR region

# Conclusions cont'd

- Most of the important bands with high $R^2$ related to bands in SWIR region and some in NIR region.
- The bands centered near 820, 1040, 1200, 1250, 1370, 1430, 1650, 2100, 2260 nm with bandwidths from 10 to 300 nm are important for constructing VIs for estimating LAI.
- The 4-point approach is a more practical application method to extract two red edge parameters because only 4 bands are considered for use
- It is notable that the originally defined VIs with R and NIR bands did not produce higher correlation with LAI than VIs constructed with bands in SWIR region.
- Atmospheric correction is critical for hyperspectral data application, especially for VNIR region

# Acknowledgments


- This research was supported by a NASA EO-1 science validation grant (NCC5-492) and field support provided by the forest plantation inventory section of the agricultural department of the government of Argentina.
- Assistance in field work by Gillsermo Defossé, Florencia Farias, and Maria Cristina Frugoni is appreciated.